The Dynamics of Static Stall

Karen Mulleners[1*], Arnaud Le Pape[2], Benjamin Heine[1], Markus Raffel[1]

1: Helicopter Department, German Aerospace Centre (DLR), Göttingen, Germany
2: Applied Aerodynamics Department, ONERA, The French Aerospace Lab, Meudon, France
* *Current address:* Institute of Turbomachinery and Fluid Dynamics, Leibniz Universität Hannover, Germany, mulleners@tfd.uni-hannover.de

Abstract The dynamic process of flow separation on a stationary airfoil in a uniform flow was investigated experimentally by means of time-resolved measurements of the velocity field and the airfoil's surface pressure distribution. The unsteady movement of the separation point, the growth of the separated region, and surface pressure fluctuations were examined in order to obtain information about the chronology of stall development. The early inception of stall is characterised with the abrupt upstream motion of the separation point. During subsequent stall development, large scale shear layer structures are formed and grow while travelling downstream. This leads to a gradual increase of the separated flow region reaching his maximum size at the end of stall development which is marked by a significant lift drop.

1 Introduction

Stall on lifting surfaces is a commonly encountered, mostly undesired, condition in aviation that occurs when a critical angle of attack is exceeded. At low angles of attack α, lift increases linearly with α. At higher angles of attack an adverse pressure gradient builds up on the airfoil's suction side which eventually forces the flow to separate and the lift to drop. The stall process comprises a series of complex aerodynamical phenomena, including transition to turbulence, shear layer instability, vortex formation, and flow separation.

In order to efficiently and effectively delay the stall process, fundamental understanding of the dynamic processes associated with stall is essential. This means that we need detailed information of the unsteady flow development and in particular of the formation and interaction of coherent structures. Only recently time–resolved particle image velocimetry (TR-PIV) became available which allows for the investigation of the development and temporal evolution of unsteady flow features. Whereas past experimental investigations generally focused on either the pre–stall or the post–stall flow, the present study provides time-resolved recordings of the velocity field and unsteady surface pressure distributions during stall development and allows for the examination of the chronology of events during stall development.

2 Experimental Set-up and Methods

Experiments consisted of TR-PIV and unsteady surface pressure measurements on a stationary two-dimensional airfoil model with an OA209 profile in a uniform subsonic flow (Mach number $Ma = 0.16$) at a free stream Reynolds number $Re = 1.8 \times 10^6$ (based on the chord length $c = 500\,\mathrm{mm}$). The airfoil model with a span of 1.4 m, yielding an aspect ratio of 2.8, was fitted into the closed test section of the F2 wind–tunnel at ONERA Toulouse, which had a rectangular cross section of $1.4\,\mathrm{m} \times 1.8\,\mathrm{m}$. TR-PIV measurements were conducted in the cross sectional plane at model mid-span. In order to achieve both a satisfying spatial and temporal resolution while covering the flow field over the entire chord length, four CMOS cameras were used simultaneously. Two of them were placed in a

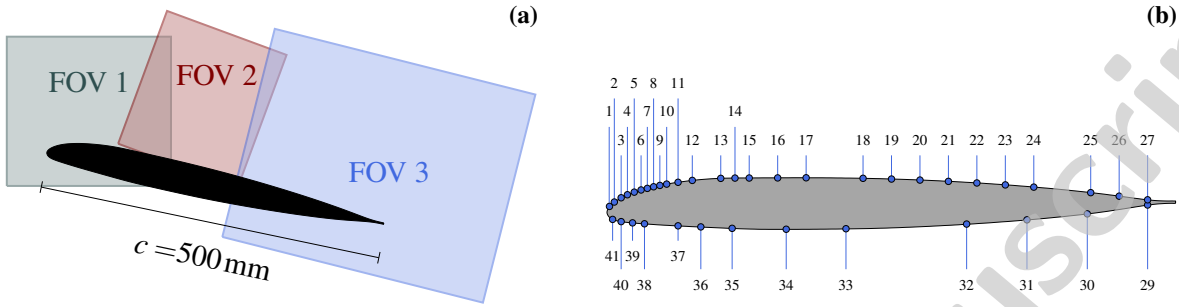

Fig. 1 Position of the PIV fields of view (a) and location of the unsteady pressure sensors in the mid-span of the OA209 airfoil section (b).

stereoscopic configuration focussing on the leading edge region (cf. *FOV 1* in figure 1). Two cameras recorded the flow in the central and the trailing edge region (cf. *FOV 2* and *FOV 3* in figure 1). Time series of 10000 frames were recorded at 2100 Hz, corresponding to an acquisition rate of 1050 Hz for the velocity fields. Synchronised with the TR-PIV, the surface pressure distribution at the model mid-span was acquired at 51.2 kHz by 37 miniature pressure transducers chordwisely distributed. The lift and pitching moment coefficient were determined by integrating the instantaneous surface pressure distributions.

To provoke a transition of the flow on the airfoil from an attached into a stalled state, the airfoil was set at an initial position with an angle of attack of approximately $\alpha = 15°$, which is slightly below the static stall angle of attack α_{ss}. Subsequently, static stall was induced by an abrupt increase of the airfoil's angle of attack beyond α_{ss} while measuring the response on the unsteady surface pressure distribution and the velocity field. This process was repeated 6 times.

To handle and explore the time–resolved flow field data, advanced post–processing techniques are required. Recently, Mulleners and Raffel (2012) combined an Eulerian vortex detection criterion (Michard et al, 1997) and a proper orthogonal decomposition (POD) (Sirovich, 1987) of the velocity field to investigate the dynamic stall development of an oscillating airfoil in a uniform subsonic flow. The same methods are used here and we refer to Mulleners and Raffel (2012) for a detailed description of the methods and their implementation.

3 Results and Discussion

Prior to tackling the dynamic processes associated with airfoil stall, we briefly discuss the general stalling characteristics of the OA209 profile.

3.1 General Stalling Characteristics

The airfoil profile considered in this study was an OA209 profile which is a typical helicopter profile with a maximum thickness of 9 %. The stationary variations of the lift and pitching moment coefficients reveal the stalling characteristics of this airfoil section at a free stream Reynolds number $Re = 1.8 \times 10^6$ (figure 2). At low angles of attack α, lift increases linearly with α and the pitching moment is negligibly small and constant. For α between 15.2° and 15.3°, the lift and pitching moments decrease abruptly. However, before maximum lift $C_{l,max} = 1.36(3)$ is reached, the lift curve is slightly rounded. This indicates a combined trailing edge and leading edge stall type (McCullough and Gault, 1951; Gault, 1957).

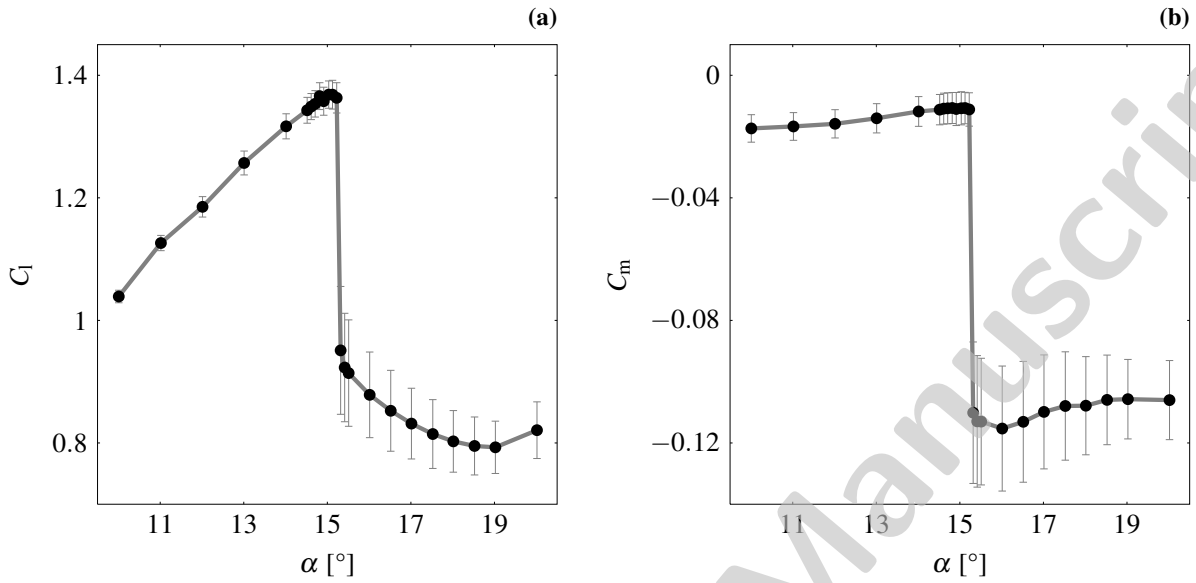

Fig. 2 Static variations of the lift (a) and pitching moment (a) coefficient with angle of attack for the OA209 and *Re* $=1.8 \times 10^6$.

3.2 Stall development

Airfoil stall was intentionally provoked by suddenly increasing the angle of attack from slightly below to immediately beyond the static stall angle of attack α_{ss}. During this transition the separating flow field and the airfoil's surface pressure distribution were measured simultaneously with a high temporal resolution allowing us to investigate the sequence of events during stall inception. Within the observation period, the angle of attack was increased from $\alpha = 15.04(1)°$ to $\alpha = 15.525(2)°$ (figure 3). In response, the lift coefficient decreased from $C_l = 1.35(2) \approx C_{l,max}$ to $C_l = 0.89(9)$, which clearly indicates the occurrence of stall. Exemplary instantaneous flow fields representing pre-stall and post-stall flow states are shown in figure 4. At pre-stall, the flow is attached for the most part

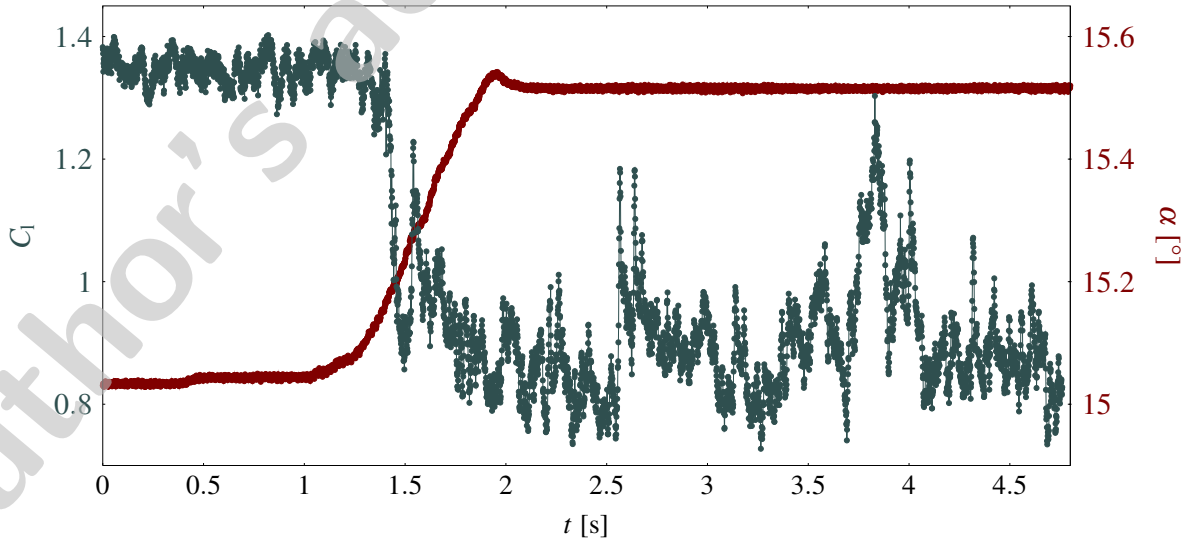

Fig. 3 Exemplary evolution of the lift coefficient and angle of attack for an intentionally stalled airfoil.

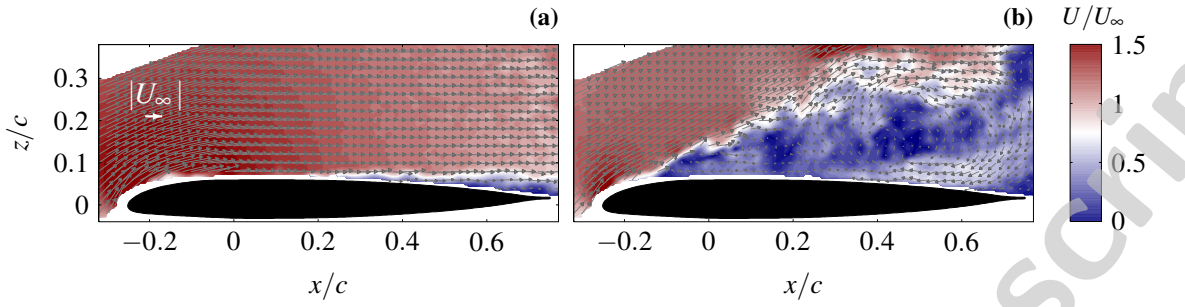

Fig. 4 Instantaneous flow fields at $\alpha = 15.06°$ (a) and $\alpha = 15.49°$ (b) representing pre-stall and post-stall flow states.

(figure 4a). There is a small recirculation region at the trailing edge, which is responsible for the decrease in lift slope near the stall angle in figure 2a. The post-stall flow field is characterised by a large separation region which starts near the leading edge (figure 4b).

As a first step towards analysing the characteristic features of stall development, we need to delimit the time period enclosing the transition from unstalled to stalled. For this purpose, we revert to the proper orthogonal decomposition (POD) method, which was used successfully by Mulleners and Raffel (2012) to determine dynamic stall onset based directly on the flow field. Here, we performed a POD of ensemble of velocity fields from 6 runs, in which the same stall provoking procedure is repeated. The spatial modes were calculated based on the ensemble of velocity field from different runs and the time development coefficients arise from the projection of the velocity field within one run on the basis formed by the spatial modes.

The first and most energetic pair of modes represent the unstalled and stalled state, respectively (figure 5a and b). The instantaneous energy contribution of these modes is indicated by the corresponding time development coefficient (figure 5c). During pre-stall, the flow field is more or less stationary and the temporal POD coefficients are approximately constant. After stall onset, the flow field is dominated by the dynamics and interaction of coherent structures and the POD coefficients show strong fluctuations. Despite these fluctuations, we can clearly distinguish two different levels for the second mode coefficient a_2, an unstalled and a stalled level. These levels are denoted by $\overline{a}_{2,\text{unstalled}}$ and $\overline{a}_{2,\text{stalled}}$, respectively, and were determined by averaging a_2 in the interval indisputably before and after stall inception. Stall development is now defined as the time period during which the flow passes from an unstalled into a stalled flow state. The starting point of stall development is specified here as the time instant at which a_2 leaves the unstalled level. Similarly, the end point is specified as the time instant at which a_2 reaches the stalled level. Mathematically, the start and end points of stall development, denoted by t_0 and t_1, are defined as

$$\begin{aligned} t_0 &= t_\text{n} \mid \forall\, t_\text{m} > t_\text{n},\ a_2(t_\text{m}) > \overline{a}_{2,\text{unstalled}} \\ t_1 &= t_\text{n} \mid \forall\, t_\text{m} < t_\text{n},\ a_2(t_\text{m}) < \overline{a}_{2,\text{stalled}} \quad . \end{aligned}$$

Stall development includes a number of unsteady flow phenomena that we are about to unravel.

3.2.1 Surface Pressure Fluctuations

When the flow on a airfoil separates, it is accompanied by large pressure fluctuations on the airfoil's surface. Considering t_0 and t_1 as the delimiters of stall development, we can compute the average surface pressure distribution and local standard deviations at pre-stall, during stall development, and at post-stall (figure 6). The large suction peak at the leading edge and the overall low pressure fluctuations at pre-stall confirm that the flow is unstalled up to t_0, while the decrease of the suction peak and

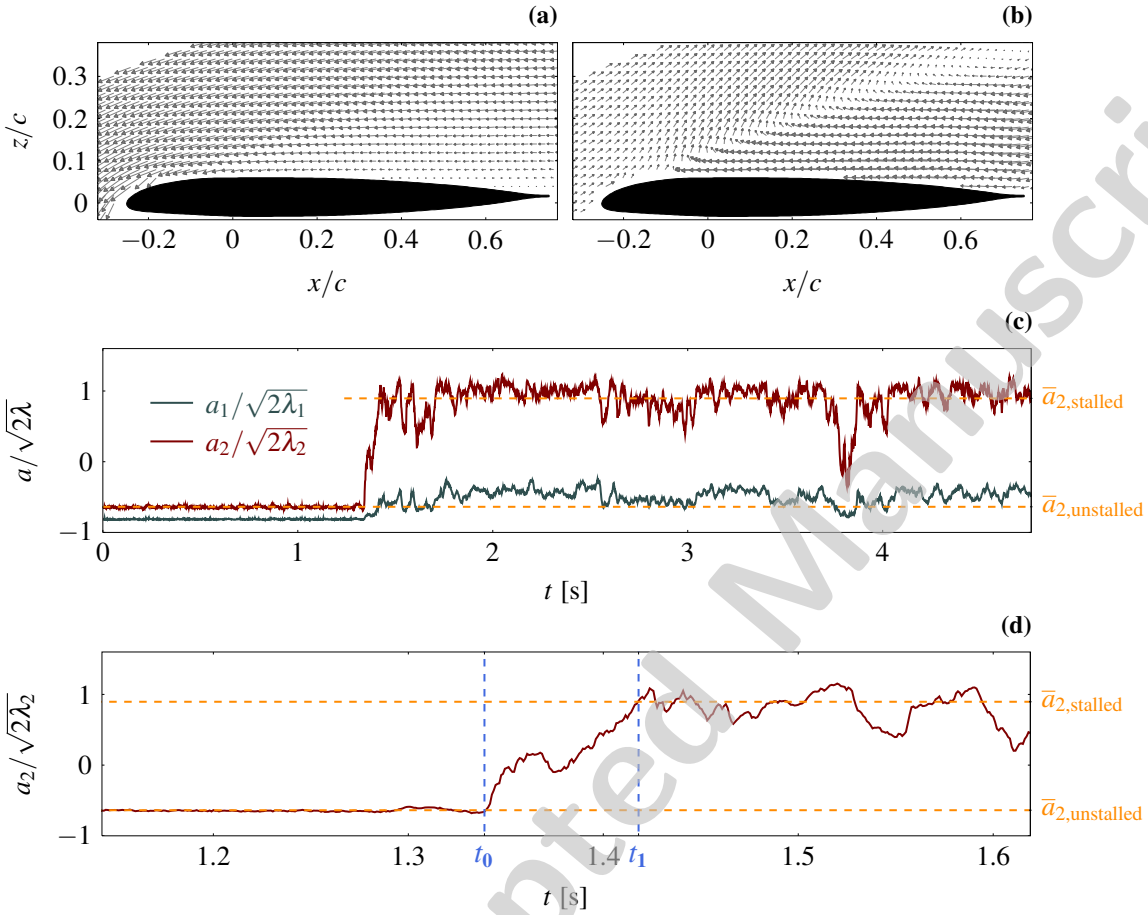

Fig. 5 First (a) and second (b) spatial modes $\psi_i(x,z)$ of the POD of the velocity field and the corresponding time development coefficients $a_i(t)$ (c). In the enlarged view of $a_2(t)$ (d), the stalled and unstalled levels and the delimiters t_0 and t_1 of stall development are indicated.

the overall increased fluctuations at post-stall indicate that the flow is indeed stalled after t_1. The location of the separation point can be determined from the average surface pressure distribution as the beginning of the constant pressure area, which occurs underneath the separated flow. At pre-stall this yields $x_{\text{sep, unstalled}}/c \approx 0.65$ and corresponds to the observation of trailing edge separation in figure 4a. The presence of coherent motion in the separated flow at the trailing edge leads to slightly higher pressure fluctuations there. Post-stall the separation point jumped upstream to $x_{\text{sep,stalled}}/c = -0.13$. The higher pressure fluctuation downstream of $x_{\text{sep,stalled}}/c$ with regard to the unstalled state are due to coherent motion in the separated flow region. The elevated pressure fluctuations upstream of $x_{\text{sep,stalled}}/c$ indicate that the separation point fluctuates and flow locally alternates between attached and separated (Simpson et al, 1981; Sicot et al, 2006). The mean surface pressure distribution associated with stall development lies in between those associated with pre- and post-stall and has the highest overall fluctuations. This confirms that the start- and endpoint of stall development determined based on the second POD mode indeed delimit the period during which the flow evolves from stalled to unstalled. Particularly interesting are the elevated fluctuations around $x/c = 0.25$ indicating unsteady flow phenomena. To identify the unsteady phenomena leading to elevated surface pressure fluctuations and to analyse in detail the movement of the separation point during stall development we revert to the velocity field data.

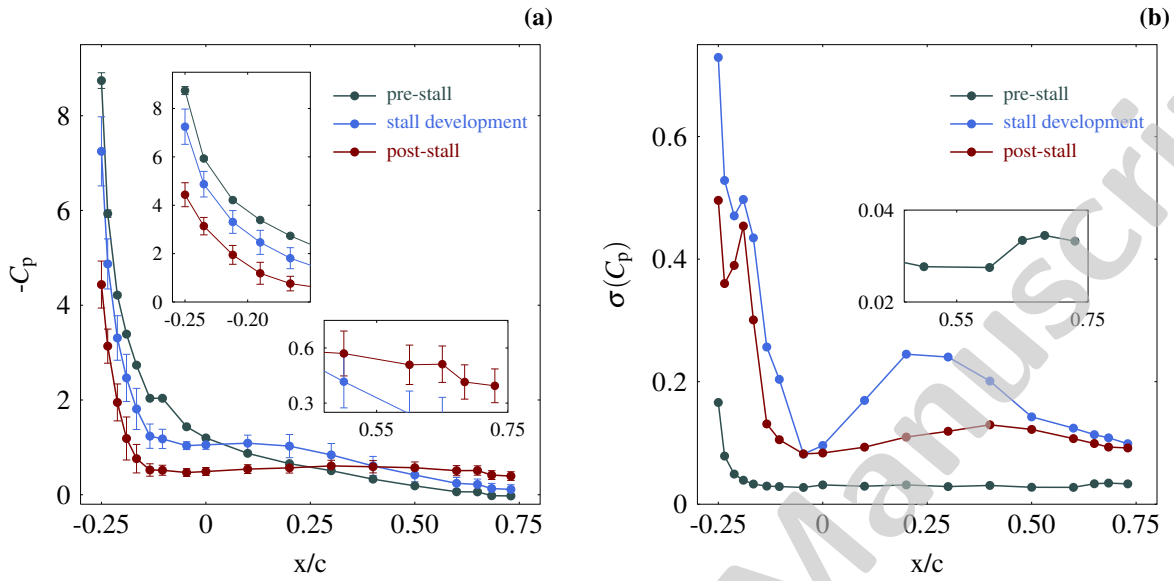

Fig. 6 Mean surface pressure distributions (a) and local surface pressure standard deviations (b) during pre-stall, post-stall, and stall development.

3.2.2 Separation Point Movement

To estimate the location of the separation point from the PIV velocity fields we consider the horizontal velocity component in the grid points closed to the airfoil's surface, i.e. along the line indicated in figure 8a. The location of the separation point is estimated by the most upstream location where backflow is observed. During pre-stall there is almost no backflow and the separation point is located near the trailing edge (figure 7a). At the very beginning of stall development, the separation point moves abruptly upstream. Within less than 20 ms the separation point moves from the leading edge to $x/c \approx 0$. In comparison, the total duration of stall development is four times longer. Due to reflections, there is no data available closer than $z = 3$ mm to the surface and the location of the separation point estimated based on PIV data is about $0.1c$ further downstream than the position estimated from the surface pressure distribution. This does not influence the conclusion that stall development starts with an abrupt upstream movement of the separation point.

3.2.3 Shear Layer Roll Up

To understand the flow development following the upstream movement of the separation point, we analyse the location and the interaction of vortices in the instantaneous velocity fields during stall development. In figure 9 instantaneous velocity fields during stall development are presented together with the positions of vortex axis determined by the Eulerian vortex detection criterion mentioned in section 2. At first, there are only positive vortices that are located in the shear layer between the free stream flow and the recirculation region near the airfoil's surface (figure 9(a)). At the beginning of stall development, the recirculation region grows and the small-scale shear layer vortices move away from the airfoil (figure 9(a)-(c)). At the same time, negative vortices emerge near the airfoil's surface and viscous interaction between the vortical structures increases. As result of these interactions the shear layer rolls up and large-scale vortices are formed. The large-scale shear layer structures are repeatedly formed at the middle of the separated zone, i.e. between $x/c \approx 0.2$ and $x/c \approx 0.4$ (figure 9(d)-(h)). This corresponds to the location where elevation surface pressure fluctuations were observed during stall development (figure 6b). At the end of stall development, the flow has reached

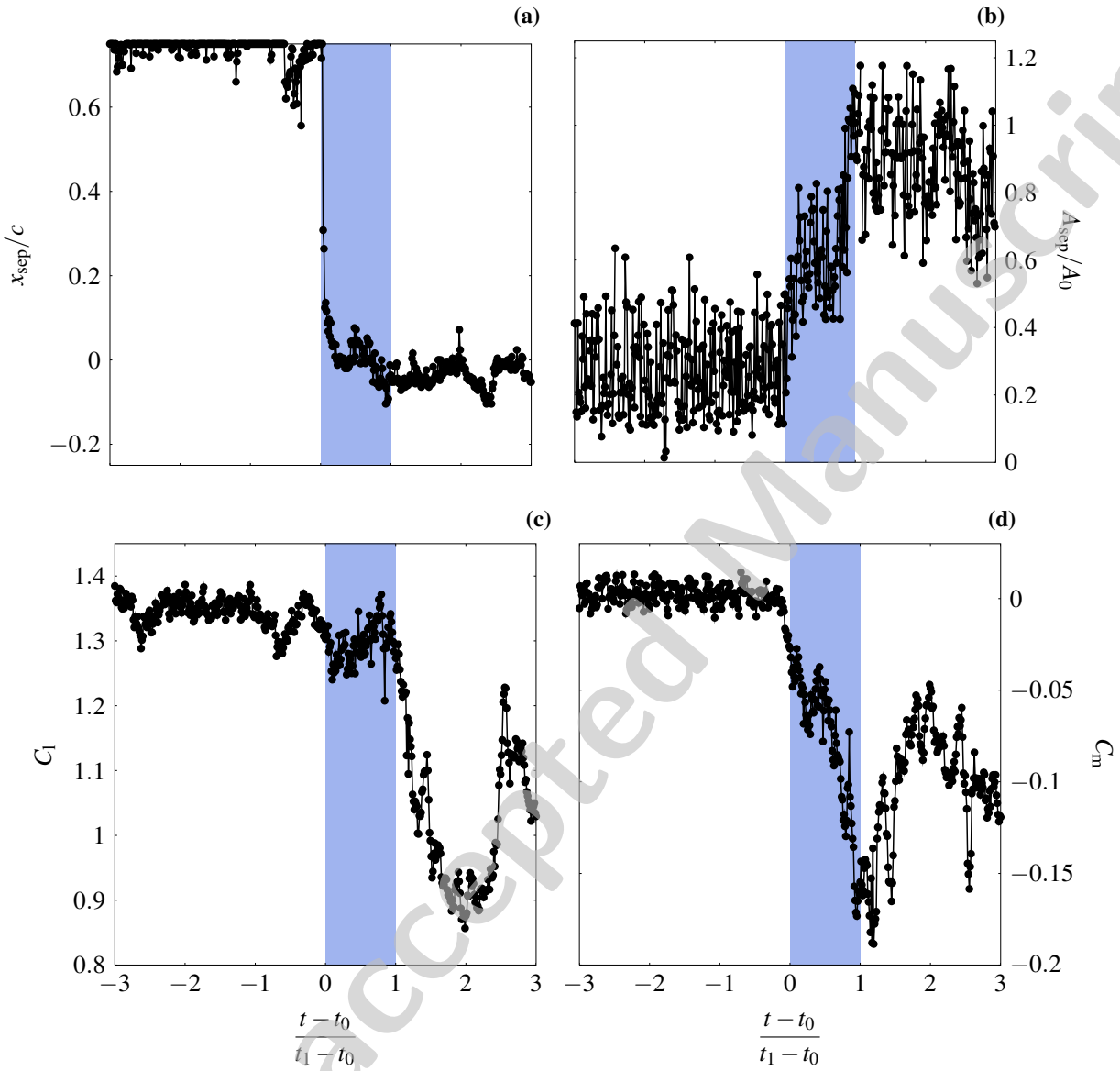

Fig. 7 Evolution of the location of the separation point (a), the size of the separated region (b), the lift coefficient (c), and the pitching moment coefficient (d) during stall development.

a fully separated state with a large region of separated flow (figure 9(j)).

Comparing the process of shear layer roll-up during static and dynamic stall development (Mulleners and Raffel, 2012), there is one important difference. During dynamic stall, the shear layer rolls up into a large scale dynamic stall vortex which grows locally and temporally, i.e. it remains in place until it has grown strong enough to separate as a result of a vortex induced separation process. Once separated, it is convected downstream and a second dynamics stall vortex can possibly be formed. This scenario of coherent structure development is generally referred to as wake mode Gharib and Roshko (1987); Hudy et al (2007). During static stall the shear layer rolls up continuously into large-scale structures that grow spatially, i.e. while travelling downstream (figure 9(g)-(i)). This scenario is similar to the flow structures development in a shear layer mode Hudy et al (2007).

To quantify the size of the recirculation or separated region, a polygon enclosing all detected vortices was determined in the individual flow fields. The area of this polygon A_{sep} was normalised

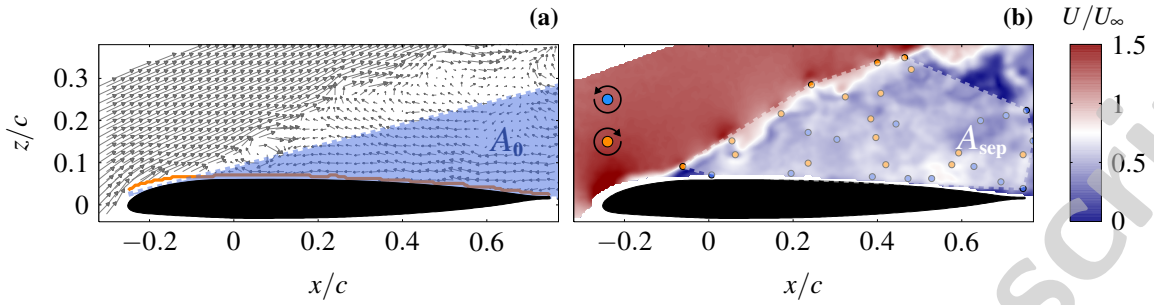

Fig. 8 Visualisation of the line closed to the airfoil's surface along which the separation point was determined and the virtual separated area that arises when the angle of attack $\alpha = 15.5°$, the separation point lies at the very leading edge, and the separation line is straight and parralel to the free stream flow (a). The size of the actual separated region was estimated as the smallest polygon enclosing all detected vortices (b).

by the area A_0. The latter represents the virtual separated area of an airfoil with angle of attack $\alpha = 15.5°$, with the separation point at the very leading edge, and assuming a straith separation line parralel to the free stream flow (figure 8a). Although this procedure is relatively rudimentary, we clearly observe an increase of the size of the separated region during stall development (figure 7b). The unstalled value represents the maximal extent of the separated flow region and is reached at the end of stall development. Furthermore, there is a strong correlation between $A_{sep}(t)$ and $C_m(t)$ during stall development and during post-stall (figure 7b and d). The lift coefficient does not show a strong correlation with either the movement of the separation nor with the size of the separated region. During stall development, lift is more or less preserved and C_l does not drop significantly until the end of stall development.

4 Conclusion

The unsteady flow dynamics during stall development on a stationary airfoil in a uniform flow were investigated by means of simultaneous, time-resolved measurements of the velocity fields and the airfoil's surface pressure distribution. Airfoil stall was intentionally provoked by suddenly increasing the angle of attack from slightly below to immediately beyond the static stall angle of attack. The start and endpoint of stall development were specified based on the temporal evolution of the second POD mode which represents a stalled flow state. The chronology of stall development starts with an abrupt upstream movement of the separation point and ends with a significant drop of the lift coefficient. In between, large-scale shear layer vortices are formed repeatedly in the middle of the separated zone leading to increased surface pressure fluctuations at that location. The spatial growth of these vortices leads to a continuously growing separation region which reaches his maximum size at the end of stall development.

Acknowledgements This work has been part of the DLR and ONERA joint project: Advanced Simulation and Control of Dynamic Stall (SIMCOS). The assistance by Jean-Michel Deluc, Thibault Joret, Philippe Loiret, Yannick Amosse and Frédéric David during the wind tunnel tests was greately appreciated.

References

Gault D (1957) A Correlation of low-speed, airfoil-section stalling characteristics with Reynolds number and airfoil geometry. Technical Note 3963, NACA

Gharib M, Roshko A (1987) The effect of flow oscillations on cavity drag. Journal of Fluid Mechanics 177:501—-530

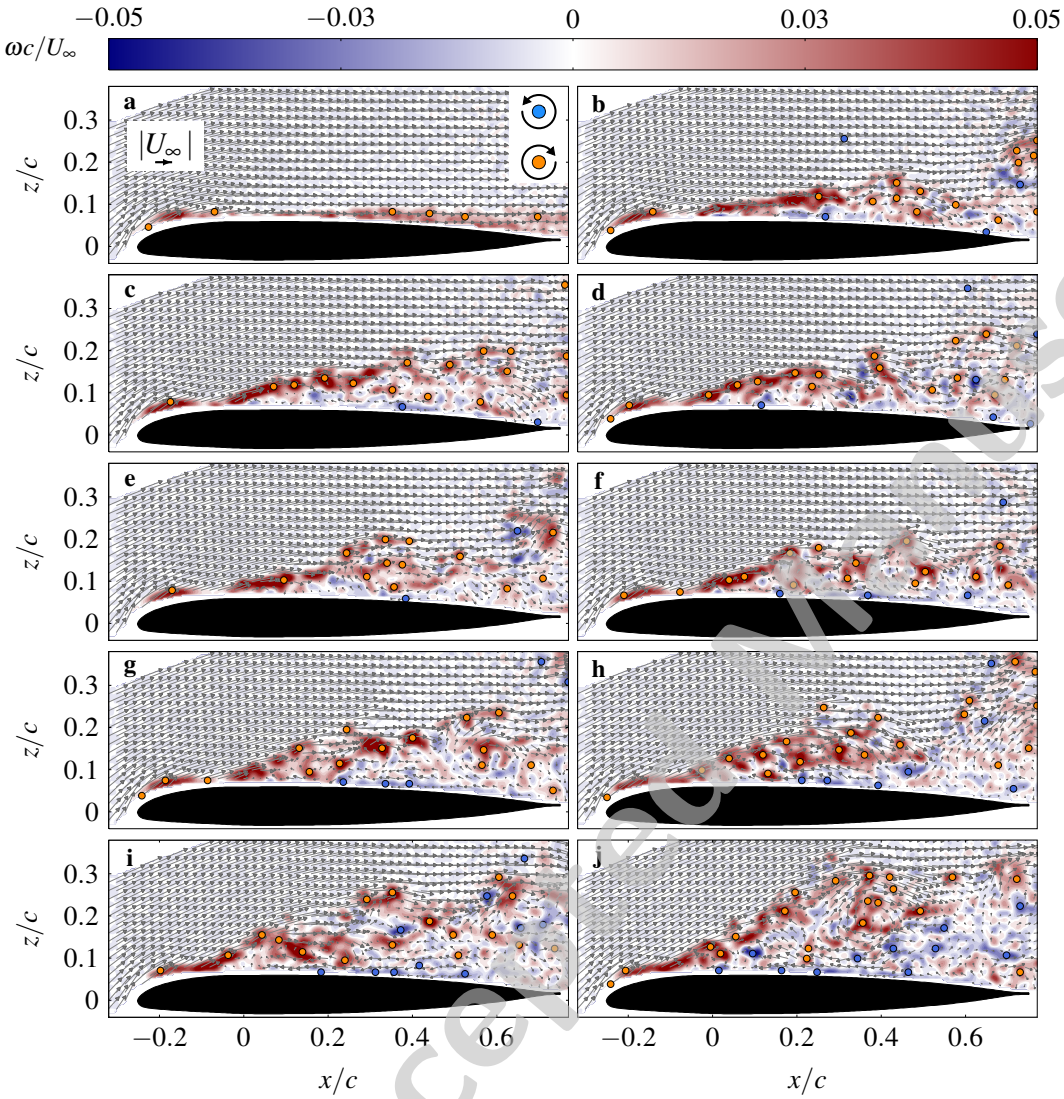

Fig. 9 Instataneous velocity and vorticity fields including the position of individual vortices at $(t-t_0)/(t_1-t_0) = -0.02$ (a), 0.12 (b), 0.27 (c), 0.41 (d), 0.55 (e), 0.64 (f), 0.72 (g), 0.81 (h), 0.89 (i), and 0.98 (j).

Hudy LM, Naguib A, Humphreys WM (2007) Stochastic estimation of a separated-flow field using wall-pressure-array measurements. Physics of Fluids 19(2):024,103, DOI 10.1063/1.2472507, URL http://link.aip.org/link/PHFLE6/v19/i2/p024103/s1\&Agg=doi

McCullough G, Gault D (1951) Examples of three representative types of airfoil-section stall at low speed. Tech. rep., NASA TN 2502

Michard M, Graftieaux L, Lollini L, Grosjean N (1997) Identification of vortical structures by a non local criterion - application to PIV measurements and DNS-LES results of turbulent rotating flows. In: Proceedings of the 11th Conference on Turbulent Shear Flows, Grenoble, France

Mulleners K, Raffel M (2012) The onset of dynamic stall revisited. Experiments in Fluids 52(3):779–793, DOI 10.1007/s00348-011-1118-y, URL http://www.springerlink.com/index/10.1007/s00348-011-1118-y

Sicot C, Aubrun S, Loyer S, Devinant P (2006) Unsteady characteristics of the static stall of an airfoil subjected to freestream turbulence level up to 16%. Experiments in Fluids 41(4):641–648

Simpson R, Chew Y, Shivaprasad B (1981) The structure of a separating turbulent boundary layer. Part 2. Higher-order turbulence results. Journal of Fluid Mechanics 113:53–73, URL http://journals.

cambridge.org/abstract_S0022112081003406
Sirovich L (1987) Turbulence and the dynamics of coherent structures; part I, II and III. Q Appl Math 45(3):561–590